Journal of Power Sources 244 (2013) 544–547

Contents lists available at SciVerse ScienceDirect

Journal of Power Sources

journal homepage: www.elsevier.com/locate/jpowsour

Short communication

Contribution of oxygen partial density of state on lithium intercalation/de-intercalation process in $Li_xNi_{0.5}Mn_{1.5}O_4$ spinel oxides

Toyoki Okumura*, Masahiro Shikano, Hironori Kobayashi

Research Institute for Ubiquitous Energy, National Institute of Advanced Industrial Science and Technology (AIST), Midorigaoka 1-8-31, Ikeda, Osaka 563-8577, Japan

HIGHLIGHTS

- Soft XANES techniques reveal the change of hybridized LUMO in $Li_xNi_{0.5}Mn_{1.5}O_4$.
- Electronic structure of O is crucial for considering redox reaction of batteries.
- Contribution of the O on redox reaction differs in various cation species.

ARTICLE INFO

Article history:
Received 25 October 2012
Received in revised form
15 January 2013
Accepted 31 January 2013
Available online 8 February 2013

Keywords:
High voltage spinel oxide
X-ray absorption fine structure
X-ray absorption near-edge structure
Lithium-ion battery

ABSTRACT

The electronic structural changes during lithium-ion intercalation/de-intercalation process of nickel substituted lithium manganese spinel oxides have been investigated by using X-ray absorption near-edge structure (XANES) spectra of O K-edges as well as Ni L_3-edges and Mn L_3-edges. The results of the XANES spectra indicate that the electronic structure of both manganese and oxygen atoms contribute on the redox reaction at $0.06 \leq x < 1$, and only that of nickel atom affect the redox reaction at $1 < x \leq 1.78$ in $Li_xNi_{0.5}Mn_{1.5}O_4$. Thus, the electronic structural change of oxygen atom is also crucial for considering redox reaction at intercalation/de-intercalation process, and the contribution of the oxygen atom on redox reaction differs in various redox cation species.

1. Introduction

A high-voltage $LiNi_{0.5}Mn_{1.5}O_4$ spinel oxide as an alternative to the conventional $LiCoO_2$ positive electrode material has been proposed to achieve higher energy density of the lithium-ion batteries since its large specific capacity above 4.5 V [1,2]. Therefore, it can be applied for electric vehicles (EV), hybrid electric vehicles (HEV), and plug-in hybrid electric vehicles (PHEV) as their power sources. The electronic structure change upon lithium-ion de-intercalation is the interest for the electrochemical behavior of $LiNi_{0.5}Mn_{1.5}O_4$ and related spinel compounds [3–9]. Terada et al. have revealed that the plateau at around 4.7 V in charge–discharge curve of the related compound $Li_{1-x}Ni_{0.31}Mn_{1.69}O_4$ was due to the redox reaction of Ni^{2+}/Ni^{4+} by using in situ X-ray absorption fine-structure (XAFS) [4]. For understanding the electrochemical properties in $Li_xNi_{0.5}Mn_{1.5}O_4$, it is also important that the fundamental study of the O 2p orbital hybridized with M 3d orbital (M are 3*d* transition metals as Ni and/or Mn) during lithium-ion de-intercalation process. Actually, in another positive electrodes, the removal/addition process of electrons from/to O 2p partial density of state (PDOS) has been investigated by soft X-ray absorption near-edge structure (XANES) techniques [10–17].

In the present paper, the change of hybridized O 2p and M 3d orbital in $Li_xNi_{0.5}Mn_{1.5}O_4$ ($0.06 \leq x < 1$) has been investigated by soft X-ray absorption near-edge structure (XANES) techniques to get the guide to understand variations of O 2p PDOS during lithium-ion de-intercalation process. We also observed the soft XANES spectra during intercalation process ($0.06 \leq x < 1$), and thereafter discuss the contribution difference of O 2p PDOS between the different redox processes.

2. Experimental

$LiNi_{0.5}Mn_{1.5}O_4$ was synthesized by the co-precipitation method [18–20]. $Ni(CH_3COO)_2 \cdot 4H_2O$ (99.9% Wako Pure Chemical Industries) and $Mn(CH_3COO)_2 \cdot 4H_2O$ (99.9% Wako Pure Chemical

* Corresponding author. Tel./fax: +81 72 751 7932.
E-mail address: toyoki-okumura@aist.go.jp (T. Okumura).

0378-7753/$ – see front matter © 2013 Elsevier B.V. All rights reserved.
http://dx.doi.org/10.1016/j.jpowsour.2013.01.189

Industries) were dissolved into distilled water, then the solution was mixed with 0.2 mol dm^{-3} NaOH solution for obtaining a hydroxide sediment. After filtering and drying, the sediment and $LiOH \cdot H_2O$ (Kojundo Chemical Laboratory) were mixed and heated at 700 °C for 18 h in air, and then cooled with a rate of 0.5 °C min^{-1}. Powder X-ray diffraction measurement (RINT-TTR) with Cu-Kα radiation equipped with a graphite monochromator was used to examine the crystal structure of resulting materials. All the XRD analyses were carried out in the Bragg–Brentano geometry mode.

To investigate electronic structures, XANES measurements of intercalated/de-intercalated samples were performed on BL4B at UVSOR II in Okazaki, Japan. An electrode was made from suspensions containing 80 wt% active material, 10 wt% acetylene black, and 10 wt% polyvinylidene difluoride, which were cast and pressed on an aluminum foil. The electrodes were assembled in a two-electrode cell using metallic lithium foil as a counter/reference electrode. A 1 mol dm^{-3} ethylene carbonate/dimethyl carbonate solution of $LiPF_6$ was used as the liquid electrolyte. Electrochemical intercalation/de-intercalation of the lithium ion was carried out at a constant current rate of 1/10 C. After stopping at each of the electrochemical reaction, the electrodes were washed by dimethyl carbonate, and then were attached to a microchannel plate detector by carbon tape. XANES spectra were recorded in a high-vacuum chamber by the total-electron-yield mode for Mn L-, Ni L- and O K-edges.

3. Results and discussion

All of the observed X-ray diffraction peaks of a pristine sample could be indexed by cubic $LiNi_{0.5}Mn_{1.5}O_4$ (space group: $P4_332$) including superlattice lines as 110, 320 [21–23]. There were no peaks of $Li_xNi_yO_2$, which has been reported as a common impurity compound [1,18,20,23]. Fig. 1 shows the electrochemical charge/discharge profile of $LiNi_{0.5}Mn_{1.5}O_4$ at 1/10 C rate. At $x < 1$ (de-intercalated process), the flat charge profile around 4.8 V vs. Li/Li^+ implies two phase reactions. The charge capacity of $LiNi_{0.5}Mn_{1.5}O_4$ is 138 mA h g^{-1}, corresponding to 94% of the lithium-ion de-intercalating from the spinel structure (the theoretical capacity when all lithium-ions are removed is 148 mA h g^{-1}). Fig. 1 also represents the curve of the derivative of the cell potential dx/dE *vs.* the composition x in $Li_xNi_{0.5}Mn_{1.5}O_4$, which indicates the two plateaus during the lithium-ion extraction as reported in the previous papers [23]. On the other hand, the flat discharge profile around 2.8 V *vs.* Li/Li^+ is observed between $x = 1.0$ and 1.5, and then the slanted discharge profile around 2.2 V *vs.* Li/Li^+ appears until $x = 1.78$ in case of a cut-off voltage of 2.0 V *vs.* Li/Li^+. The circles in Fig. 1 indicate the various intercalated/de-intercalated states of $Li_xNi_{0.5}Mn_{1.5}O_4$ samples for XANES measurements. The values of x in $Li_xNi_{0.5}Mn_{1.5}O_4$ were calculated by assuming that all electric currents were utilized for the lithium-ion intercalated/de-intercalation process.

The Mn L-edge spectra at various lithium contents (Fig. 2(a)) consisted of two parts of peaks *ca.* 10 eV separated: L_3 and L_2 appear at around 643 eV and 653 eV, respectively [11–13,16,17,24]. These peaks correspond to electronic transitions from the $2p_{3/2}$ and $2p_{1/2}$ sites to an unoccupied 3d state. The L_2-edge peaks are broader than those of the L_3-edge peaks. This difference has been explained by Coster–Kronig Auger decay [24], that is, there is a shorter lifetime of the $2p_{1/2}$ core hole due to a radiationless electron transition from the $2p_{3/2}$ to the $2p_{1/2}$ level, accompanied by the excitation of a valence electron into the conduction band. Several groups have used the L_3-edge features of $Mn^{4+}O_2$ (peaks a and b) and $Mn_2^{3+}O_3$ (peaks c′ and d′) to determine the valence state of Mn in $LiMn_2O_4$ (Mn^{3+}/Mn^{4+}) (Fig. 2(b)) [11,16]. Compared with the report in $LiMn_2O_4$, the peaks c′ and d′ are almost disappeared in the L_3-edge feature of pristine electrode $LiNi_{0.5}Mn_{1.5}O_4$ [16], that means that the valence state of Mn in prepared $LiNi_{0.5}Mn_{1.5}O_4$ is close to Mn^{4+}. It should be noted that the little swelling of the peaks c′ and d′ was observed. The small amounts of Mn^{3+} species exist in pristine electrode even for low rate cooling during synthesis. This is in good

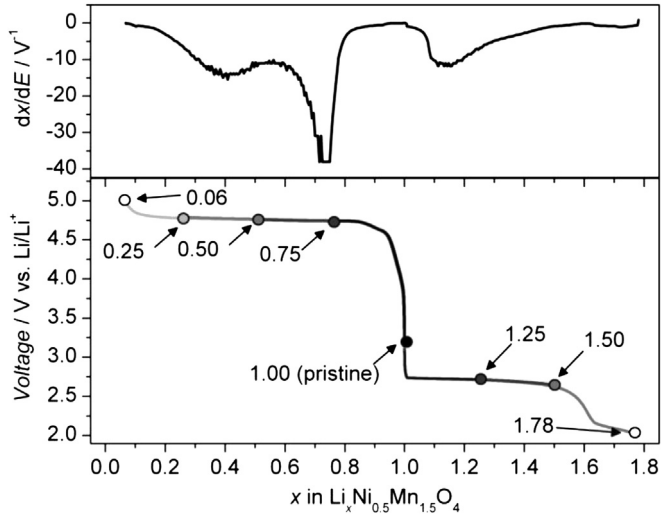

Fig. 1. Lithium-ion intercalation/de-intercalation behavior in $Li_xNi_{0.5}Mn_{1.5}O_4$ spinel oxide. Circles indicate lithium content of samples measured by XANES spectra.

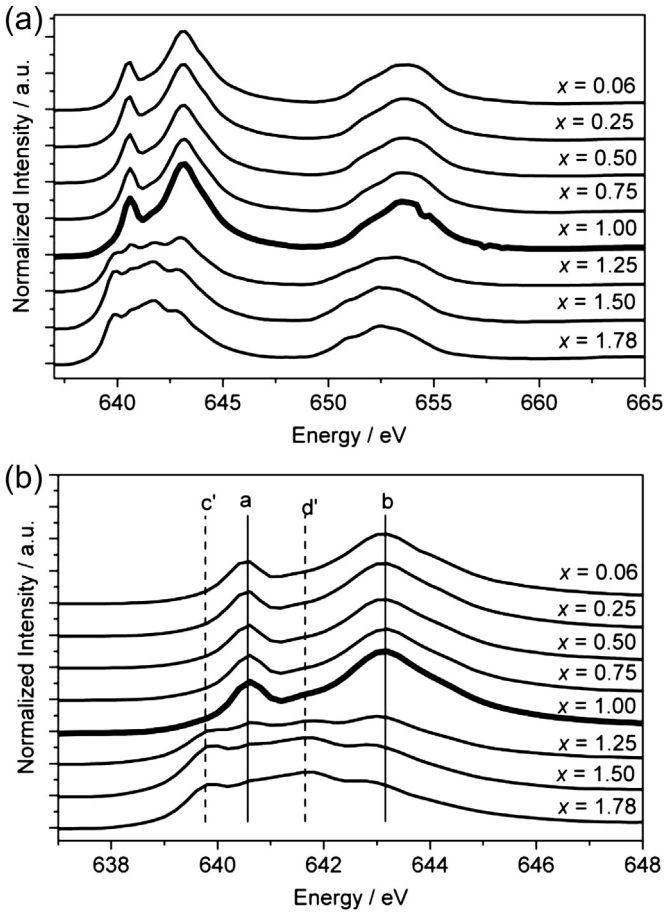

Fig. 2. XANES spectra of Mn L_3-edges in $Li_xNi_{0.5}Mn_{1.5}O_4$.

agreement with the Mn K-edge XANES result of $Li_{1-x}Ni_{0.31}Mn_{1.69}O_4$ reported by Terada et al. [4]. The absorption edge energy of Mn L_3-edge peaks shift toward lower energy levels and the intensity ratio of peaks c′ and d′ to peaks a and b increases with an increase of lithium content x in the range of $1 < x \leq 1.78$, while the absorption edge peaks are unchanged in the range of $0.06 \leq x < 1$. This result indicates that the charge variation at the discharge profile around 2.8 and 2.2 V *vs.* Li/Li^+ was compensated by the redox reaction of the Mn^{3+}/Mn^{4+} couple. On the other hand, the Mn 3d orbital does not contribute to the discharge profile around 4.8 V *vs.* Li/Li^+ [4]. The L_3-edge spectra of Mn^{3+} and Mn^{4+} in $Li_xNi_{0.5}Mn_{1.5}O_4$ ($1 < x \leq 1.78$) are also similar to the L_3-edge calculated ones summarized by de Groot et al. [24], using atomic multiplet theory with inclusion of the cubic octahedral (O_h) crystal field.

The Ni L-edge spectra at various lithium contents (Fig. 3(a)) consist of two parts of peaks: L_3 ($2p_{3/2} \rightarrow 3d$) and L_2 ($2p_{1/2} \rightarrow 3d$) appeared at around 854 and 869 eV, respectively [12–15,24,25]. The valence state of Ni in $LiNi_{0.5}Mn_{1.5}O_4$ ($x = 1$) is approximately 2+ because its L_3-edge spectrum (which consists of major peak a and minor peak b) is similar to the calculated ones of Ni^{2+} compounds having the octahedral (O_h) crystal field [24,25]. The absorption edge energy of Ni L_3-edge peaks is unchanged in the range of $1 < x \leq 1.78$, and thus the Ni 3d orbital does not contribute on the discharge profile around 2.8 and 2.2 V *vs.* Li/Li^+. Besides that, the intensity ratio of peaks a and b is greatly changed with an increase of lithium content x in the range of $0.06 \leq x < 1$. The L_3-edge spectra at $x = 0.50$, 0.25, and 0.06 are gradually close to the calculated one of the low spin Ni^{3+} reported by van Elp et al. [25] and the experimental ones of Ni^{3+} and Ni^{4+} in other Ni complexes [26]. These results indicate that the valence state variation during lithium-ion de-intercalation at the charge profile around 4.8 V *vs.* Li/Li^+ was compensated by the redox reaction of the Ni^{2+}/Ni^{4+} couple via Ni^{3+}. This is also in good agreement with the Ni K-edge XANES result of $Li_{1-x}Ni_{0.31}Mn_{1.69}O_4$ [4]. Thus, the large voltage gap between $x < 1$ and $x > 1$ in Fig. 1 results from the difference potential of ions.

The O *K*-edge XANES spectra of $Li_xNi_{0.5}Mn_{1.5}O_4$ at various lithium contents x are shown in Fig. 4(a). These spectra show the transitions from the O 1s core orbital to the unoccupied O 2p orbital according to the dipole transition selection rules. Moreover, the O 2p orbital hybridizes with transition-metal 3d and 4sp orbitals. Therefore, the absorption peaks in the O K-edge XANES spectra reflect an unoccupied O 2p orbital character hybridized with the transition-metal 3d and 4sp orbitals [27]. Broad peaks around 535–550 eV are concerned with the transition from O 1s orbital to the hybridized orbital among O 2p, M 4sp and Li 2sp PDOS. The left shoulders of the broad peaks decrease with the reducing of lithium ion contents x since the contribution of Li 2sp PDOS to the hybridized orbital decreases, which confirmed by the DFT calculation [28]. The main peaks a and b, which were observed at around 528–534 eV, can be assigned to the transitions from O 1s orbital to the hybridized orbital between O 2p orbital and M 3d orbital (Fig. 4(b)). The peaks a and b particularly indicate the transition from O 1s to hybridized orbital of O 2p with M 3d t_{2g} and that of O 2p with M 3d e_g, respectively [11]. Furthermore, the decrement of the peak area around 528–535 eV with lithium-ion insertion until $x \leq 1.78$ indicates that the transition probability to unoccupied hybridization orbital decreases with the electrochemical redox reaction of Mn^{3+}/Mn^{4+} in $Li_xNi_{0.5}Mn_{1.5}O_4$: the area of the first peak decreases, and

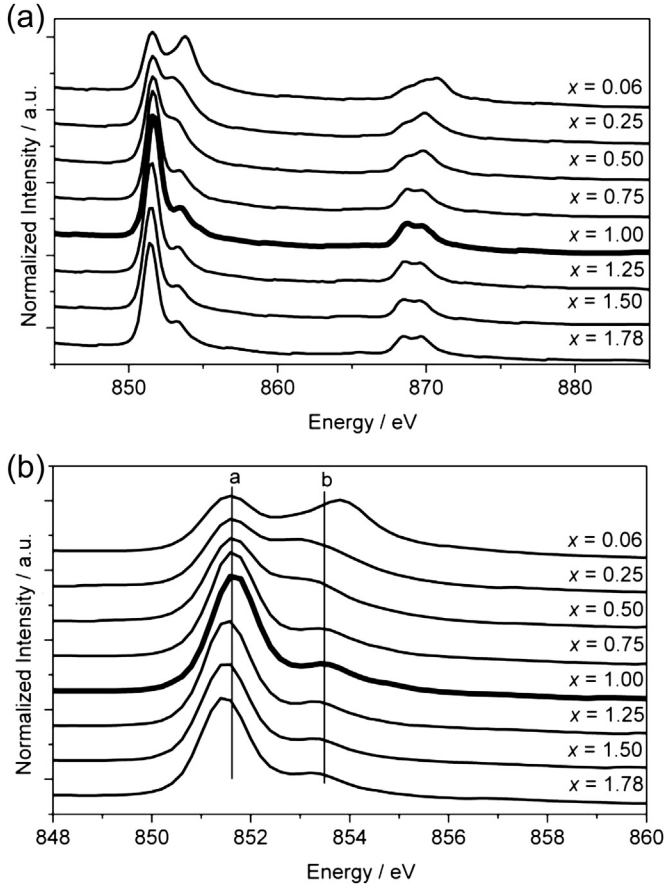

Fig. 3. XANES spectra of Ni L_3-edges in $Li_xNi_{0.5}Mn_{1.5}O_4$.

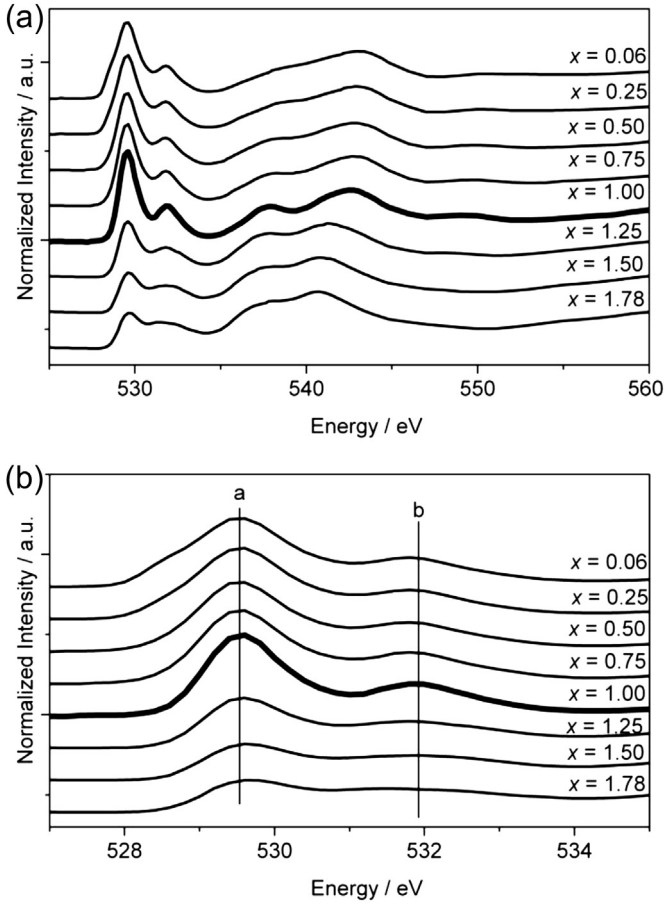

Fig. 4. XANES spectra of O K-edges in $Li_xNi_{0.5}Mn_{1.5}O_4$.

the area of the peak b becomes broader. Two types of metal–ligand interaction have been commonly proposed for transition-metal oxides to discuss the contribution of O 2p PDOS. One is a charge-transfer (CT) type whereby the energy transfers a ligand electron to a hybridization state of M 3d orbital and O 2p orbital. The other is a Mott–Hubbard (MH) type, whereby the energy simply transfers a ligand electron to the metal ion. This result strongly suggests that the electronic structure of $Li_xNi_{0.5}Mn_{1.5}O_4$ is a CT type or an intermediate between CT and MH regimes. On the other hand, the peak area around 528–535 eV is unchanged during lithium-ion de-intercalation until $x \geq 0.06$, in which the electrochemical redox reaction occurs by the redox reaction of Ni^{2+}/Ni^{4+}. This results from that the electronic structure of $Li_xNi_{0.5}Mn_{1.5}O_4$ is an MH type. Therefore, the contribution of O 2p PDOS on electrochemical reaction has been changed with the elements and valence states of cations. It would be considered that Mn 3d PDOS is strongly hybridized with O 2p PDOS, and both Mn L-edge and O K-edge XANES spectra are changed during lithium-ion intercalation until $x \leq 1.78$. On the other hand, Ni 3d PDOS is not overlapped with O 2*p* PDOS, that is localized to, and only Ni L-edge XANES spectra are changed during lithium-ion de-intercalation until $x \geq 0.06$. Our findings would provide fundamental information for understanding lithium-ion intercalation/de-intercalation reaction.

4. Conclusion

In order to get the guide to improve the superior electrochemical properties, the detailed electronic structural changes in $Li_xNi_{0.5}Mn_{1.5}O_4$ during lithium-ion intercalation/deintercalation process were determined by soft XANES spectra. At $x < 1$, the absorption edge peak at the right shoulder of Ni L_3-edge peaks clearly appeared with the decrement of the lithium-ion contents although the significant change could not be observed in Mn L_3-edge peaks. On the other hand, at $x > 1$, the absorption edge energy of Mn L_3-edge peaks shifted toward lower energy levels with an increase of lithium content while Ni L_3-edge peaks were mostly maintained. The large voltage gap between $x < 1$ and $x > 1$ in Fig. 1 results from the difference of the redox-ion species.

The absorption edge peaks of the O K-edge spectra indicate the transition from O 1s to O 2p orbital hybridized with transition-metal 3d. At $x > 1$, the shape of the peaks changed with the increase of the lithium content as well as the shape of Mn L_3-edge peaks changes as written above, although it maintained at $x > 1$. These results indicated that both manganese and oxide ions contributed on the redox reaction at $x < 1$, and only nickel ion affects the redox reaction at $x > 1$. Thus, the electronic structural change of oxide ion is also crucial for considering redox reaction in charge/discharge batteries, and the contribution of the O 2p PDOS on redox reaction differs in various redox cation species.

References

[1] Q. Zhong, A. Bonakdarpour, M. Zhang, Y. Gao, J.R. Dahn, J. Electrochem. Soc. 144 (1997) 205.
[2] T. Ohzuku, S. Takeda, M. Iwanaga, J. Power Sources 81–82 (1999) 90.
[3] B. Ammundsen, D.J. Jones, J. Rozière, F. Villain, J. Phys. Chem. B 102 (1998) 7939.
[4] Y. Terada, K. Yasaka, F. Nishikawa, T. Konishi, M. Yoshio, I. Nakai, J. Solid State Chem. 156 (2001) 286.
[5] S.-J. Hwang, H.-S. Park, J.-H. Choy, G. Campet, J. Phys. Chem. B 105 (2001) 335.
[6] H. Shigemura, H. Sakaebe, H. Kageyama, H. Kobayashi, A.R. West, R. Kanno, S. Morimoto, S. Nasu, M. Tabuchi, J. Electrochem. Soc. 148 (2001) A730.
[7] W. Wen, B. Kumarasamy, S. Mukerjee, M. Auinat, Y. Ein-Eli, J. Electrochem. Soc. 152 (2005) A1902.
[8] D.H. Park, S.T. Lim, S.-J. Hwang, J.-H. Choy, J.H. Choi, J. Choo, J. Power Sources 159 (2006) 1346.
[9] M. Womes, P.E. Lippens, B. León, C. Pérez-Vicente, J.L. Tirado, J. Power Sources 175 (2008) 570.
[10] Y. Uchimoto, H. Sawada, T. Yao, J. Synchrotron Radiat. 8 (2001) 872.
[11] S. Kobayashi, T. Usui, H. Ikuta, Y. Uchimoto, M. Wakihara, J. Am. Ceram. Soc. 87 (2004) 1002.
[12] W.-S. Yoon, M. Balasubramanian, X.-Q. Yang, Z. Fu, D.A. Fischer, J. McBreen, J. Electrochem. Soc. 151 (2004) A246.
[13] W.-S. Yoon, M. Balasubramanian, K.Y. Chung, X.-Q. Yang, J. McBreen, C.P. Grey, D.A. Fischer, J. Am. Chem. Soc. 127 (2005) 17479.
[14] W.-S. Yoon, K.Y. Chung, J. McBreen, D.A. Ficher, X.-Q. Yang, J. Power Sources 163 (2006) 234.
[15] W.-S. Yoon, K.Y. Chung, J. McBreen, D.A. Fischer, X.-Q. Yang, J. Power Sources 174 (2007) 1015.
[16] C.T. Meneses, F.C. Vicentin, J.M. Sasaki, M.A. Macêdo, J. Electron Spectrosc. Relat. Phenom. 156–158 (2007) 326.
[17] T. Okumura, T. Fukutsuka, K. Matsumoto, Y. Orikasa, H. Arai, Z. Ogumi, Y. Uchimoto, Dalton Trans. 40 (2011) 9752.
[18] Y. Fan, J. Wang, X. Ye, J. Zhang, Mater. Chem. Phys. 103 (2007) 19.
[19] X. Fang, N. Ding, X.Y. Feng, Y. Lu, C.H. Chen, Electrochim. Acta 54 (2009) 7471.
[20] R. Snathanam, B. Rambabu, J. Power Sources 195 (2010) 5442.
[21] Y. Idemoto, H. Nakai, N. Koura, J. Power Sources 119–121 (2003) 125.
[22] J.-H. Kim, S.-T. Myung, C.S. Yoon, S.G. Kang, Y.-K. Sun, Chem. Mater. 16 (2004) 906.
[23] K. Ariyoshi, Y. Iwakoshi, N. Nakayama, T. Ohzuku, J. Electrochem. Soc. 151 (2004) A296.
[24] F.M.F. de Groot, J.C. Fuggle, B.T. Thole, G.A. Sawatzky, Phys. Rev. B 42 (1990) 5459.
[25] J. van Elp, B.G. Searle, G.A. Sawatzky, M. Sacchi, Solid State Commun. 80 (1991) 67.
[26] H. Wang, P. Ge, C.G. Riordan, S. Brooker, C.G. Woomer, T. Collins, C.A. Melendres, O. Graudejus, N. Bartlett, S.P. Cramer, J. Phys. Chem. B 102 (1998) 8343.
[27] F.M.F. de Groot, J. Faber, J.J.M. Michiels, M.T. Czyzyk, M. Abbate, J.C. Fuggle, Phys. Rev. B 48 (1993) 2074.
[28] T. Okumura, Y. Yamaguchi, M. Shikano, H. Kobayashi, J. Mater. Chem. 22 (2012) 17340.